Atmos. Chem. Phys. Discuss., 15, 27219–27251, 2015
www.atmos-chem-phys-discuss.net/15/27219/2015/
doi:10.5194/acpd-15-27219-2015

Atmospheric Chemistry and Physics Discussions
Open Access

Detecting moisture transport pathways to the subtropical North Atlantic free troposphere using paired H_2O-δD in situ measurements

Y. González[1,2], M. Schneider[3], C. Dyroff[3], S. Rodríguez[2], E. Christner[3], O. E. García[2], E. Cuevas[2], J. J. Bustos[2], R. Ramos[2], C. Guirado-Fuentes[2], S. Barthlott[3], A. Wiegele[3], and E. Sepúlveda[2]

[1]Sieltec Canarias, S. L., Hábitat 2, 38204, San Cristóbal de La Laguna, Santa Cruz de Tenerife, Islas Canarias, Spain
[2]Izaña Atmospheric Research Centre (IARC), Agencia Estatal de Meteorología (AEMET), Santa Cruz de Tenerife, Islas Canarias, Spain
[3]Institute of Meteorology and Climate Research (IMK-ASF), Karlsruhe Institute of Technology (KIT), Karlsruhe, Germany

Received: 13 August 2015 – Accepted: 14 September 2015 – Published: 8 October 2015

Correspondence to: Y. González (ygonzalezr@aemet.es)

Published by Copernicus Publications on behalf of the European Geosciences Union.

Abstract

We present two years of measurements of water vapour (H_2O) and its isotopologue ratio (δD, the standardized ratio between $H_2{}^{16}O$ and $HD^{16}O$) made at two remote mountain sites on Tenerife Island in the subtropical North Atlantic. We show that the data – if measured during nighttime – are well representative for the lower/middle free troposphere. We use the measured H_2O-δD pairs, together with dust measurements and back-trajectory modelling for analysing the moisture pathways to this region. We can identify four principally different transport pathways. The first two pathways are linked to transport from high altitudes and high latitudes, whereby the respective air can be dry, due to last condensation occurring at low temperatures, as well as humid, due to cross isentropic mixing with lower level and more humid air during transport since last condensation. The third pathway is transport from lower latitudes and lower altitudes, whereby we can identify rain re-evaporation as an occasional source of moisture. The fourth pathway is linked to the African continent, where during summer dry convection processes over the Sahara very effectively inject humidity from the boundary layer to higher altitudes. This so-called Saharan Air Layer (SAL) is then advected westward over the Atlantic and contributes to moisten the free troposphere. We demonstrate that different pathways leave distinct fingerprints on the measured H_2O-δD pairs.

1 Introduction

In the subtropical free troposphere, in the region of the descending branch of the Hadley cell, the humidity is not conserved along the mean subsidence (Pierrehumbert, 1998). Instead, this dry air is often moistened (Galewsky and Hurley, 2010; Couhert et al., 2010; Risi et al., 2012). The few studies based on atmospheric modelling points the turbulent transport of water vapour from the surface upward as the dominant moistening process balancing the drying in the subtropical free troposphere (Couhert et al., 2010; Risi et al., 2012). Additional processes, such us evaporation of condensate and isentropic eddy transport of moist air from the tropics, are suggested to also contribute to moist this region (Galewsky and Hurley, 2010, and references therein); but the sources and dynamics involved in this moistening are still unclear.

Several studies indicate that water vapour isotopologue observations are very promising for investigating the different moisture pathways in this region, such observations can be used to distinguish between the different mechanisms associated to the moistening (e.g., Galewsky and Hurley, 2010; Noone et al., 2011; Kimberly et al., 2014; Dyroff et al., 2015; Schneider et al., 2015). However, so far, works related to continuous high quality in situ water isotopologues measurements have not been reported.

In this paper, we present and discuss the first multi-year observational in situ data set of free tropospheric water vapour isotopologues from the subtropics. In the following we express the isotopologues $H_2{}^{16}O$ and $HD^{16}O$ as H_2O and HDO. The δ-notation expresses the per mil difference of the stable isotopic composition of a water sample ($R = HDO/H_2O$) from that of the isotope ratio of Vienna Standard Mean Ocean Water, i.e., $\delta D = 1000 \times (R/R_{VSMOW} - 1)$ ($R_{VSMOW} = 3.1152 \times 10^{-4}$, Craig, 1961).

In Sect. 2 of this paper we present the measurement sites and discuss the methodology of our study. In Sect. 3 we document that our nighttime measurements are representative for the subtropical North Atlantic lower free troposphere. We use backward trajectories and dust measurements as tracers for detecting the main meteorological processes. Then, we document that these processes leave unique fingerprints in the H_2O-δD distribution. Section 4 resumes the work.

2 Methodology

2.1 Measurement site

As study area we use Tenerife (Canary Islands, Spain; 28.3° N, 16.5° W). At this island, two high mountain sites are run by the Izaña Atmospheric Research Centre. IZO is a mountain top station located at 2367 m a.s.l., whereas TDE is a small measurement

ACPD
15, 27219–27251, 2015

Title Page
Abstract | Introduction
Conclusions | References
Tables | Figures
◀I | ▶I
◀ | ▶
Back | Close
Full Screen / Esc
Printer-friendly Version
Interactive Discussion

site located at the volcanic cone at 3550 m a.s.l. In the context of the project MUSICA (MUlti-platform remote Sensing of Isotopologues for investigating the Cycle of Atmospheric water), we installed two Picarro instruments at IZO and TDE stations. These instruments provide continuous isotopologues data for altitudes above 2000 m which are unique for the subtropical North Atlantic.

A schematic depiction of the locations of IZO and TDE and the meteorological processes affecting the measurement sites is shown in Fig. 1. In the subtropical North Atlantic region, the atmospheric stability is determined by the combination of two synoptic processes that well define the Marine Boundary Layer (MBL) and the Free Troposphere (FT). In the MBL, a quasi-permanent North-northeast (NNE) trade wind blows (< 1000 m a.s.l., Palmén and Newton, 1969). In the FT, the descendent branch of the Hadley cell around 30° N results in a North-west (NW) subsidence regime (Galewsky et al., 2005; Cuevas et al., 2013). This subsidence is frequently alternated in summer with South-east (SE) Saharan dust outbreaks (Chiapello et al., 1999). Episodes of airmass transport from from South-west (SW) direction are also occasionally observed.

The local moisture exchange between the MBL and the FT is limited by a Temperature Inversion Layer (TIL). In the surroundings of the island, the top of the MBL, which is frequently located just below the TIL, is characterized by a stratocumulus layer formed by condensation of water vapour onto the pre-existing particles (Rodríguez et al., 2009). This layer creates a quasi-continuous foggy and rainy regime between 800 and 2000 m a.s.l., that is more pronounced on the northern part of the island. The effectiveness of the TIL in separating the MBL from the FT is reflected in the relative humidity (RH) profile. In the FT, the RH is typically around 20 %; while is normally above 60 % in the MBL (Cuevas et al., 2013). Vertical mixing between MBL and FT air is observed during daylight due to the upslope flow regimen.

2.2 Measurements of water vapour isotopologues

Two commercial cavity ring-down spectrometers (Picarro model L2120-I) have been used for water vapour isotopologues monitoring at the two mountain sites at Tenerife.

ACPD
15, 27219–27251, 2015

At IZO, measurements started in March 2012, and at TDE in July 2013. Time series of H_2O and δD (around 2 years of 10 min average) at IZO and TDE stations are shown in Figs. 2 and 3 (left column), respectively. The measurement gaps are due to instrument failure and maintenance.

The instruments are calibrated every 8–12 h by using liquid standards injected with Picarro's Standard Delivery Module (SDM). The absolute uncertainties of the δD measurements are < 13.7‰ at 500 ppmv and < 2.3‰ at 4500 ppmv. The error estimation accounts for instrument precision as well as errors due to the applied data corrections (SDM effects + instrumental drifts < 1‰, uncertainties of liquid standards < 0.7‰, and calibration < 0.5‰ for δD). More detailed information about the calibration procedure and stability of the two instruments is given in Appendix A.

2.3 Measurements of dust

Long-term measurements of aerosol at Izaña includes chemical composition, dust concentrations and size distribution. The methodology and quality control of aerosol in situ techniques are described in Rodríguez et al. (2012). In Izaña, bulk mass concentrations of aerosols is clearly dominated by desert Saharan dust (Basart et al., 2009; Rodríguez et al., 2011). We used records of dust at Izaña to detect the arrival of North African air (Rodríguez et al., 2012).

Unfortunately, in situ dust measurements are not available at TDE. In order to distinguish between clean and dust laden conditions at this station we use the AERONET columnar-integrated aerosol optical depth (AOD) level 2.0 obtained at a wavelength of 500 nm at IZO (http://aeronet.gsfc.nasa.gov). See more details of calibration procedures, data acquisition and processing in Guirado et al. (2014).

2.4 Back-trajectories

Transport pathways of moisture are analysed by integrating the Global Data Assimilation System archive information (GDAS1, NCEP) in the Hybrid Single Particle Lagrangian Integrated Trajectory model HYSPLIT 4.0. The GDAS1 is available each 6 h, and the post-processing converts the data to 1° × 1° latitude–longitude grids and from sigma levels to the 23 pressure levels between 1000 and 20 hPa (Rolph et al., 2014). HYSPLIT performs a linear interpolation between the times of the available input data (6 h) for calculating 5 day back-trajectories (Draxler and Rolph, 2003). The vertical component of the back-trajectories was computed using the vertical model velocity. The end points of the trajectories were set at Tenerife (28.3° N, 16.5° W) at the elevations of the IZO and TDE stations.

3 Results

3.1 The effect of diurnal upslope flow

The airflow regime at IZO is driven by the occurrence of upward transport of humid air during daylight and downward transport of dry FT air at night. The upward transport is caused by the combination of the thermally driven growth of the MBL volume and the buoyant airflows caused by the heating of the air located just above the terrain (Rodríguez et al., 2009). This upslope flow prompts the climb of gases emitted at lower parts of the island, which is captured in the marked daily cycle of gases and particles measured at IZO (e.g., Rodríguez et al., 2009). The highest concentrations of pollutants is observed in the early afternoon.

The right columns in Figs. 2 and 3 show the monthly mean daily cycle of H_2O and δD at IZO and TDE stations, respectively. There is a marked daily cycle in the H_2O and δD data of the IZO station (Fig. 2) and a weaker one at the TDE station (Fig. 3). At IZO, the diurnal cycle of H_2O and δD is more pronounced than the annual cycle. At TDE, the H_2O annual cycle is stronger than the diurnal cycle. However, at TDE, δD data also show a diurnal cycle with an amplitude similar to the amplitude of the annual cycle.

The distribution of the 10 min H_2O-δD pairs collected at IZO and TDE stations are shown in Fig. 4. The whole data set is presented in grey dots; black dots show the data collected at night (from midnight to 1 h after sunrise) and orange crosses show the data collected during daylight (from 3 to 10 h after sunrise, when the upslope breeze is active). At IZO, the lowest δD values are measured at nighttime (left column in Fig. 4). During daylight, we observe less depletion. The H_2O-δD pairs measured at IZO during daylight are assembled in the upper side of the H_2O-δD distribution ($\delta D = -146 \pm 39$‰, orange crosses, left column in Fig. 4). At midday, the increase of humidity is associated to a mean isotopic composition of $\delta D = -131 \pm 35$‰. This value is similar to the one measured close to the ocean by Dyroff et al. (2015, $\delta D = -124 \pm 43$‰ around the top of the MBL, 600–900 m a.s.l.). Thus, the shifting of the H_2O-δD pairs to the upper side of the distribution is the result of the mixing of dry FT air with water evaporated from the surrounding ocean and exported by turbulent mixing at the top of the MBL. This result is in agreement with those found by Noone et al. (2011) in Mauna Loa (Hawaii).

At TDE, the difference between the daylight and nighttime H_2O-δD distribution is not as clear as at IZO (right column in Fig. 4). The weaker diurnal effect at TDE station is due to its location. TDE is located at a higher altitude on a rather sharp peak (Pico del Teide). There it is less exposed to the slope breezes, and consequently, the influence of the MBL-FT air mixing is weaker.

At IZO, gases and particles measured at nighttime well represent FT conditions (Gómez-Peláez et al., 2006; Rodríguez et al., 2009, 2012; Cuevas et al., 2013). To examine the variability of the H_2O-δD pairs in the subtropical North Atlantic FT, and in order to avoid the possible local MBL-FT mixing, only the H_2O-δD pairs measured at nighttime at IZO and TDE will be considered in the following study.

3.2 The Saharan Air Layer and the moisture in the subtropical North Atlantic FT

The meteorological pattern of the subtropical North Atlantic region is characterized by a constant transport of Atlantic airmasses that alternates with Saharan dust events, especially in summer. Previous works carried out in this region show that these two regimes can easily be distinguished by their dust content. At IZO, dust concentrations under background clean conditions are lower than $2\,\mu g\,m^{-3}$ (Rodríguez et al., 2009); whereas during Saharan events, dust concentrations above $25\,\mu g\,m^{-3}$ are usually observed (Rodríguez et al., 2015). The Izaña AOD levels for background conditions are usually lower than 0.05 (García et al., 2012), and frequently above 0.10 during dust events (Basart et al., 2009; García et al., 2012).

The left column in Figs. 5 and 6 show the distribution of 5 day back-trajectories for non-dust and dust laden conditions at IZO and TDE stations, respectively. We considered that an airmass experiences condensation when RH along the trajectory to the station exceeds the limit of 80 % during at 3 h time interval (James et al., 2004; Sodemann et al., 2008). If this occurs, we set this point as initial point of the back-trajectory. If no condensation was observed along the 5 days path, the back-trajectory was fully drawn. Clean dust-free airmasses originate from the FT over the Atlantic (first row in Figs. 5 and 6). Dust laden airmasses are originated in North Africa close to the surface (dust $> 25\,\mu g\,m^{-3}$, AOD > 0.1, second row in Figs. 5 and 6).

The right column in Figs. 5 and 6 show the 10 min average H_2O-δD pairs measured under non-dust (green dots) and dust laden conditions (red dots) at IZO and TDE stations, respectively. The whole H_2O-δD distribution (grey dots) is quite well confined within two theoretical curves. The theoretical line on the low δD value side of the distribution represents the evolution of an airmass that has experienced Rayleigh distillation, a gradual dehydration over the ocean, in which all condensate is removed during adiabatic cooling (initial conditions: RH = 80 % and SST = 25 °C, orange line). The theoretical line on the high δD side of the distribution models the moistening by evap-

ACPD
15, 27219–27251, 2015

oration from the ocean surface (initial conditions of airmass 1: $H_2O = 18\,mmol\,mol^{-1}$, $\delta D = -84$ ‰; airmass 2: $H_2O = 0.4\,mmol\,mol^{-1}$, $\delta D = -600$ ‰, black solid line). These theoretical lines mostly cover the set of H_2O-δD measured during this study.

The H_2O-δD pairs associated to clearly non-dust conditions represent 55 % of the data collected at IZO, and 51 % of the data collected at the TDE. The origin of the North Atlantic airmasses reaching IZO and TDE stations covers a wide area (0–60° N, 45° W–20° E), and also a wide range of altitudes (0–10 km; left column in Figs. 5 and 6). A wide H_2O-δD distribution is measured under the arrival of dust-free airmasses (green dots in right column in Figs. 5 and 6). This distribution illustrates the effect of non-Rayleigh processes affecting H_2O and δD, such as airmass mixing and different H_2O-δD-relations (Rayleigh-curves) of airmasses from different source regions (Brown et al., 2013). At both stations, nighttime H_2O-δD pairs below a minimum Rayleigh curve for airmasses with subtropical origin (initial $H_2O = 27\,mmol\,mol^{-1}$, $\delta D = -71$ ‰) cannot be explained by condensation or mixing. Therefore, this occasional super-Rayleigh observations indicate additional fractionation related to either intracloud or subcloud processes or postcondensational exchange (Brown et al., 2013, and references therein).

Saharan dust conditions (dust $> 25\,\mu g\,m^{-3}$) were observed in 20 % of IZO and 19 % of TDE of the whole recorded data. At IZO summer data represent 74 % of the Saharan dust measurements, and 70 % of TDE measurements. The H_2O-δD pairs collected under dust laden conditions were confined in the upper part of the distribution (red dots in Figs. 5 and 6). During these events, relatively enriched and moist H_2O-δD pairs were measured. Mean values for IZO were -133 ± 35 ‰ and $7 \pm 3\,mmol\,mol^{-1}$; and for TDE -152 ± 44 ‰ and $5 \pm 2\,mmol\,mol^{-1}$, respectively. The H_2O-δD distribution under dust laden events is well limited by theoretical lines that simulate the mixing between BL and FT air. The dashed black line drawn in Figs. 5 and 6, represents the mixing between the following airmasses: airmass (1) $H_2O = 16\,mmol\,mol^{-1}$, $\delta D = -93$ ‰ and airmass (2) $H_2O = 0.4\,mmol\,mol^{-1}$, $\delta D = -600$ ‰. This mixing line was determined as best fit of the border of the data of dust laden air.

ACPD
15, 27219–27251, 2015

Episodes of moderate dust content ($2 < \text{dust} < 25\,\mu\text{g}\,\text{m}^{-3}$, $0.02 < \text{AOD} < 0.1$) are related to airmasses that have travelled westward from the African continent towards the Atlantic Ocean and then return eastward laden with remaining dust where they are measured at IZO. These events are the mixing product of clean North Atlantic and Saharan dust laden airmasses. As consequence, they do not show a unique fingerprint on the H_2O-δD distribution, and they are not shown here.

Dust-laden Saharan airmasses contribute to moisten the dry subtropical North Atlantic FT. The information of the H_2O-δD pairs measured under these conditions indicate typical dehydration/mixing process also observed over the ocean. The transport of dust starts over the Sahara desert, where dust storms are driven by local thermal low pressure systems at the surface. In summer, the shift northward of the north-east trade winds and the Inter-Tropical Convergence Zone (ITCZ) in combination with a convective boundary layer prompts the strong injection of dust at high altitudes (Rodríguez et al., 2015). The dust is then exported westward at subtropical latitudes (20–30° N) within the Saharan Air Layer (SAL), a stratum of warm dust laden air, normally located between an altitude of 1 to 5 km with a maximum dust load at an altitude between 2 and 3 km (e.g., Prospero et al., 2002; Rodríguez et al., 2011; Andrey et al., 2013; Rodríguez et al., 2015). Previous works indicate that the moisture content of the SAL during summer has its origin on the evaporation of the warmer Mediterranean Sea, which is then driven by the trade winds over the Sahara, mixed with dust and then transported into the SAL to the subtropical North Atlantic FT (Millán et al., 1997, 2004; Rodríguez et al., 2011).

3.3 Moisture transport over the North Atlantic Ocean

In this section, we focus on the moisture transport pathways over the North Atlantic. For this purpose, we only work with airmasses corresponding to clean conditions (not linked to SAL) and we use the theory of the last condensation (LC) point. According to this theory, the mixing ratio is determined by the specific humidity at the point of LC,

ACPD
15, 27219–27251, 2015

in case it is not affected by subsequent mixing (Galewsky et al., 2005, and references therein).

We use GDAS1 data and HYSPLIT back-trajectories to derive information about the LC point and mixing after LC and then relate this information to our H_2O-δD observations. The LC point is identified at the area where RH exceeds 80 % during a 3 h time interval (James et al., 2004; Sodemann et al., 2008). We use the corresponding 3 h averages of temperature and specific humidity at this LC point (in the following referred to as T_{LC} and H_2O_{LC}) for classifying the airmasses.

We create three different data groups: $T_{LC} < 250$ K, $250\,K < T_{LC} < 270$ K, and $T_{LC} > 270$ K. The temperatures $T_{LC} = 250$ K and $T_{LC} = 270$ K correspond to humidities of approximately 1.7 and 8 mmol mol^{-1}, respectively. The top panels of Fig. 7 (left for IZO and right for TDE) show that T_{LC} is a good proxy for the locations of the LC point. The coldest saturation temperatures (220–250 K, blue colour) typically corresponds to air transported from the upper extra-tropical troposphere (> 40° N, < 450 hPa). These airmasses represent 32 and 43 % of the airmasses reaching IZO and TDE station, respectively. Airmasses experiencing LC at warmer temperatures (250–270 K) usually originate between 20 and 50° N at 400–600 hPa (grey colour in Fig. 7). They represent 48 and 42 % of the airmasses reaching IZO and TDE, respectively. Warmest LC temperatures (270–290 K) usually originate between 0 and 40° N and pressure levels above 600 hPa (red colour in Fig. 7). They represent 20 and 14 % of the airmasses reaching IZO and TDE, respectively.

We use the logarithmic difference between the humidity given by GDAS1/HYSPLIT at the station ($H_2O_{t=0}$) and the humidity at the LC point (H_2O_{LC}), in order to analyse if the airmass experienced variations on the moist content during the transport from the LC point to the stations ($\log[H_2O_{t=0}] - \log[H_2O_{LC}]$, hereafter ΔH_2O). We postulate that the airmasses with ΔH_2O within the ±0.1 bin do conserve the properties of the LC point during their transport to IZO and TDE. Negative ΔH_2O indicates that the airmasses mix with drier airmasses during the transport to the stations (we exclude situations of rainout by requiring that RH never reaches 80 % before the LC point).

ACPD
15, 27219–27251, 2015

Positive ΔH_2O indicates that the airmasses get moister. The bottom panels of Fig. 7 shows the normalized distribution of ΔH_2O for the three T_{LC} groups (blue, black, and red coloured lines, respectively). Left panel for IZO and right panel for TDE.

At IZO the humidity concentrations since the LC point are best conserved for $T_{LC} > 250$ K (red and grey line). At TDE we observe a reasonable conservations for $T_{LC} < 270$ K (grey and blue line) and a generally a drying for airmasses with $T_{LC} > 270$ K (red line). The total contribution of airmasses with $\Delta H_2O < -0.1$ (i.e. drying since LC) is 19 % at IZO and 43 % at TDE, revealing that drying by mixing with dry air is more frequently observed at IZO than for TDE. For T_{LC} (> 270 K), i.e. for air that has been rather humid at the LC point the drying by mixing with subsiding dry air is very clearly observed at TDE (red line, bottom right panel of Fig. 7). The total contribution of airmasses with $\Delta H_2O > +0.1$ (i.e. moistening since LC) is 46 % at IZO and 29 % at TDE. This moistening is most pronounced for air with the LC point in the upper troposphere of the extra-tropics ($T_{LC} < 250$ K) and it becomes in particularly evident at IZO (blue line, bottom left panel of Fig. 7). This moistening process is more important at IZO than at TDE, due to IZO's location at a lower altitude, which is directly affected by turbulent mixing from the marine boundary layer.

Figure 8 shows the H_2O-δD distribution as measured at IZO for the different T_{LC} groups. The H_2O-δD data pairs correspond to 10 min averages measured within ±3 h of the airmass arrival time of the trajectory. For each T_{LC} group, the H_2O-δD data points have been colour-coded as a function of ΔH_2O. The green colour highlights those data associated to ΔH_2O within ±0.1, thus, conserving water vapour concentrations since LC. The orange colour marks data with ΔH_2O out of the ±0.1 range. Figure 9 shows the same for TDE station.

For the cold LC temperatures ($T_{LC} < 250$ K) and at TDE we typically observe dry air ($H_2O < 3\,\mathrm{mmol\,mol^{-1}}$, see left panels in Fig. 9). For IZO we also observe dry air if there has been no mixing since LC ($\Delta H_2O \pm 0.1$, green dots, upper left panel in Fig. 8). However, this is only the case for about 14 % of all the airmasses that have their LC at these low temperatures. Generally at IZO the humidity is not conserved since LC if T_{LC}

ACPD
15, 27219–27251, 2015

is low. In most cases these airmasses are mixed with humid air during their transport. This mixing can then be observed in the measured H_2O-δD pairs. If there is a lot of mixing ($H_2O > 8\,\mathrm{mmol\,mol^{-1}}$) the vapour is clearly enriched in HDO, which is consistent with moistening by mixing with humid air (orange dots in the bottom left panel of Fig. 8).

For the warmest LC temperature group ($T_{LC} > 270\,\mathrm{K}$, right panels in Fig. 8) we observe occasionally H_2O-δD pairs below the exemplary Rayleigh distribution, which can be explained by evaporation from a rather warm Ocean or by re-evaporation of falling rain droplets. Under these conditions the subtropical North Atlantic free troposphere is particularly humid. Mixing with air from higher atmospheric levels can dry these airmasses. Such mixing since LC manifests in H_2O-δD pairs above the exemplary Rayleigh line, in particularly if there is strong mixing ($H_2O < 3\,\mathrm{mmol\,mol^{-1}}$, orange dots in bottom right panels of Figs. 8 and 9).

For airmasses linked to intermediate T_{LC} (above 250 and below 270 K; central column in Figs. 8 and 9) we observe a mix of the different processes as discussed above.

It is important to keep in mind that the meteorological parameters upwind of the stations as deduced by HYSPLIT/GDAS1 are the result of a dispersion model and analysis fields, each with an uncertainty. It is likely that our analyses is affected by these uncertainties. Nevertheless, we are able to demonstrate a clear relation between the HYSPLIT/GDAS1 data and the measured H_2O-δD pairs which a posteriori justifies our approach. Our simplified analysis suggests that the distribution of the moisture in the subtropical North Atlantic FT is controlled by the temperature at last condensation and subsequent mixing of airmasses. Thus, these results are in agreement with the idealized advection-condensation model proposed by Galewsky and Hurley (2010).

4 Summary and conclusions

We report continuous measurements of water vapour isotopologues made at two mountain observatories (IZO at 2370 m and TDE at 3550 m a.s.l.) on the Island of Tenerife. We assume that the measurements made in the second half of the night are only very weakly affected by the local circulation on the island, and are well representative for the FT. This assumption is consistent to previous studies of trace gases made on the island's mountain and it is also consistent to the wide distribution of the H_2O-δD pairs corresponding to the nighttime observations. Thus, our measurements generate a unique continuous water vapour isotopologue data record for the lower/middle FT and can be used for studying free tropospheric water pathways. For such study we combine the isotopologue data with back-trajectory calculations and dust measurements.

The distribution of water vapour isotopologues collected during dust-free North Atlantic conditions show a wide variability. This variability has been analysed in the context of the last condensation point. The results show that the most depleted δD values registered at IZO are found in relation to airmasses that have experienced condensation at lower temperatures at higher latitudes and altitudes over the North Atlantic Ocean ($T_{LC} < 250$ K, $> 40°$ N, < 400 hPa). The condensation at low temperatures is responsible for the dryness of the subtropical North Atlantic FT. These airmasses seem to frequently experience mixing with more humid airmasses during the transport to the subtropical region. Moistening during subsidence was detected by analysing GDAS1/HYSPLIT data and identified in the measured H_2O-δD distribution. Airmasses experiencing last condensation close to the surface at lower latitudes and especially in the surroundings of the Canaries (> 270 K, > 600 hPa) were detected. In this region, rain re-evaporation or evaporation over a warm Ocean can be identified in the H_2O-δD distribution (increased depletion with respect to Rayleigh).

For dust episodes, rather humid and enriched vapour is detected at the stations, indicating indicate a strong injection of boundary layer air into the FT. These dust laden airmasses, product of a strong convection over the Sahara desert, reach the Canaries without having experienced significant condensation, and are found as an influential contribution of moistening in this region. We show that the measurements of water vapour isotopologues at regions located to the West of the African continent provide new insights into the influence of the African continent on the moisture budget of the FT of the subtropical Northern Atlantic.

ACPD
15, 27219–27251, 2015

In summary, our results indicate that, four different moisture transport pathways have to be considered in order to understand the subtropical North Atlantic moisture budget. While the dominant dryness of the region is determined by the mean subsidence of dry air from high altitudes of the extra-tropics (pathway 1), there are three main processes that moisten the FT over the Atlantic: horizontal mixing over the Atlantic with air from the Saharan Air Layer (pathway 2), transport of air from low altitudes ($P > 600$ hPa) and latitudes (whereby humidity occasionally originates from rain-evaporation, pathway 3), and vertical mixing close to the Canaries (pathway 4).

Figure 10 gives an overview on the H_2O-δD distributions as observed when one of the four different pathways is clearly prevailing. It depicts the areas with highest density of the observed H_2O-δD pairs. Pathway 2 is dominating when there is high aerosol load (dust $> 25\,\mu g\,m^{-3}$ or AOD > 0.1, red contour lines). The other pathways are dominating for low aerosol load (dust $< 2\,\mu g\,m^{-3}$ or AOD < 0.02) and when T_{LC} and ΔH_2O are situated within specific ranges. Pathway 1 is prevailing for $T_{LC} < 250$ K and ΔH_2O within ± 0.1 (grey contour lines). Pathway 3 is prevailing for $T_{LC} > 270$ K and ΔH_2O within ± 0.1 (green contour lines). Finally pathway 4 is dominating for $T_{LC} < 250$ K and $\Delta H_2O > 1.0$ (blue contour lines). This pathway is mainly limited to altitudes below 3000 m a.s.l., and it is more frequently observed at IZO than at TDE.

The summary as shown in Fig. 10 reveals that the H_2O-δD pairs measured in the subtropical North Atlantic FT well reflect the dominating moisture transport pathways to this atmospheric region. A continued long-term monitoring of water vapour isotopologue ratios would offer a unique possibility for investigating the importance of the different mechanisms responsible for the expected moistening of the subtropical North Atlantic FT in response to climate change.

Appendix A: Calibration procedure of PICARRO instruments

A1 Mixing ratio calibration

Measurements of absolute humidity obtained from the meteorological sensors have been used for correcting Picarro's humidity measurements. The meteorological stations are located close to respective Picarro inlets. The temperature and relative humidity of these stations have been used for calculating the water vapour pressure ($e = e_{sat} \cdot \mathrm{RH}/100$). The saturation vapour pressure is calculated from the Magnus–Tetens formula ($e_{sat} = 6.1094 \cdot \exp^{(17.625 \cdot T)/(243.04+T)}$, WMO, 2008).

Figure A1 shows 10 min resolution of simultaneous measurements of humidity from the meteorological station and the Picarro at IZO and TDE stations, respectively. The slope (S), intercept (i) and coefficient of determination (r^2) of the linear fit at each station are shown. The linear fit obtained at each station is applied as a correction for the whole humidity measurements.

A2 Isotopic calibrations with the SDM system

The isotopic calibration is carried out every 8–12 h by measuring two liquid standards of composition $\delta \mathrm{D}_{S1} = -142.2 \pm 0.7$ ‰ and $\delta \mathrm{D}_{S2} = -245.3 \pm 0.7$ ‰. These two standards are reasonably representative for the situation at IZO and TDE. In order to correct the humidity dependence, these two standards are analysed periodically at three different water vapour mixing ratios (around 6, 12 and 18 $\mathrm{mmol\,mol^{-1}}$). The time intervals between sampling and calibration, as well as the calibration humidity points have been slightly modified as a function of the demands in certain campaign periods. The calibration procedure takes 2 h.

The calibration steps are generated by mixing the different liquid sample volumes with a synthetic air flow. At TDE, the air flow is controlled by an electronic mass flow controller, while at IZO, the flow is controlled by a rotameter. The reduced precision of

ACPD
15, 27219–27251, 2015

this second device is translated in a bigger variability of the fixed humidity points at IZO in comparison with the TDE (Fig. A2).

The isotopic calibration starts by filtering those data recorded in the transition between sampling and calibration, in the transition between the 3 humidity calibration points, as well as those related to clogged syringes. The left column in Fig. A2 shows the difference between the Picarro δ-readings obtained during the SDM calibration at the 3 humidity points (standard 1 is shown in blue dots and standard 2 in black dots) at the 2 stations. No significant differences are observed along the humidity range covered with the SDM, being the 2σ below 2‰ (instrumental precision < 0.5‰). Each day, the data are calibrated with the resulting combination of the calibration at 3 different humidity points (no humidity dependence was found) and a linear fit between the responses of the 2 standards. The time series of the SDM calibrations carried out at IZO and TDE stations are shown in the right column in Fig. A2 (gaps are due to instrumentation's repairs). No temporal drifts are observed in the different time series indicating that both Picarro instruments are very stable and consistent over time.

The SDM calibration is appropriate for the humidity ranges were the SDM works properly (6000–25 000 ppmv). To characterize the Picarro response for lower humidities, an experiment with a gas bubbler covering a humidity until 500 ppmv, was carried out in our lab right after the installation under controlled temperature conditions. This exercise showed no humidity dependences on the Picarro's isotopologues readings, but more variability. From that experiment, we use the SDM calibration procedure for the whole range of humidity measured at the stations considering the following absolute uncertainties in δD: < 13.7‰ at 500 ppmv and < 2.3‰ at 4500 ppmv. The error estimation accounts for instrument precision as well as errors due to the applied data corrections (SDM effects + instrumental drifts < 1‰, liquid standard bias < 0.7‰, calibration bias < 0.5‰ for δD).

Acknowledgements. This study has been conducted in the framework of the project MUSICA (MUlti-platform remote Sensing of Isotopologues for investigating the Cycle of Atmospheric water) funded by the European Research Council under the European Community's Seventh

Framework Programme (FP7/2007-2013/ ERC Grant agreement number 256961). We thank Dan Smale (NIWA, New Zealand) and the staff of Arrival Heights/Scott Base for providing the Antarctic ice water probes we used for preparing our isotopologue standards. The isotopologue composition of the probes was kindly determined by LSCE-CEA, France. Aerosol measurements are part of the project POLLINDUST (CGL2011-26259) funded by the Minister of Economy and Competitiveness of Spain. The AERONET sun photometer at Izana (PI: Emilio Cuevas) has been calibrated within AERONET EUROPE TNA supported by the European Community Research Infrastructure Action under the FP7 Capacities program for Integrating Activities, ACTRIS grant agreement number 262254. Eliezer Sepúlveda is supported by the NOVIA project (Ministerio de Economía y Competitividad of Spain, CGL2012-37505).

References

Andrey, J., Cuevas, E., Parrondo, M., Alonso-Pérez, S., Redondas, A., and Gil-Ojeda, M.: Quantification of ozone reductions within the Saharan air Layer through a 13-year climatologic analysis of ozone profiles, Atmos. Environ., 84, 28–34, doi:10.1016/j.atmosenv.2013.11.030, 2013. 27228

Basart, S., Pérez, C., Cuevas, E., Baldasano, J. M., and Gobbi, G. P.: Aerosol characterization in Northern Africa, Northeastern Atlantic, Mediterranean Basin and Middle East from direct-sun AERONET observations, Atmos. Chem. Phys., 9, 8265–8282, doi:10.5194/acp-9-8265-2009, 2009. 27223, 27226

Brown, D., Worden, J., and Noone, D.: Characteristics of tropical and subtropical atmospheric moistening derived from Lagrangian mass balance constrained by measurements of HDO and H_2O, J. Geophys. Res., 118, 54–72, doi:10.1029/2012JD018507, 2013. 27227

Chiapello, I., Prospero, J., Herman, J., and Hsu, N.: Detection of mineral dust over the North Atlantic Ocean and Africa with the Nimbus 7 TOMS, J. Geophys. Res., 104, 9277–9291, doi:10.1029/1998JD200083, 1999. 27222

Couhert, A., Schneider, T., Li, J., Waliser, D. E., and Tompkins, A. M.: The maintenance of the relative humidity of the subtropical free troposphere, J. Climate, 23, 390–403, doi:10.1175/2009JCLI2952.1, 2010. 27220

Craig, H.: Standard for Reporting concentrations of Deuterium and Oxygen-18 in natural waters, Science, 13, 1833–1834, doi:10.1126/science.133.3467.1833, 1961. 27221

ACPD

15, 27219–27251, 2015

Moisture pathways and H_2O-δD pairs in the subtropical North Atlantic free troposphere

Y. González et al.

Cuevas, E., González, Y., Rodríguez, S., Guerra, J. C., Gómez-Peláez, A. J., Alonso-Pérez, S., Bustos, J., and Milford, C.: Assessment of atmospheric processes driving ozone variations in the subtropical North Atlantic free troposphere, Atmos. Chem. Phys., 13, 1973–1998, doi:10.5194/acp-13-1973-2013, 2013. 27222, 27225

Draxler, R. and Rolph, G.: HYSPLIT (HYbrid Single-Particle Lagrangian Integrated Trajectory) Model Access Via NOAA ARL READY, NOAA Air ReSOURCEs Laboratory, Silver Spring, MD Website, available at: http://www.arl.noaa.gov/ready/hysplit4.html (last access: June 2015), 2003. 27224

Dyroff, C., Sanati, S., Christner, E., Zahn, A., Balzer, M., Bouquet, H., McManus, J. B., González-Ramos, Y., and Schneider, M.: Airborne in situ vertical profiling of $HDO/H_2{}^{16}O$ in the subtropical troposphere during the MUSICA remote sensing validation campaign, Atmos. Meas. Tech., 8, 2037–2049, doi:10.5194/amt-8-2037-2015, 2015. 27221, 27225

Galewsky, J. and Hurley, J. V.: An advection-condensation model for subtropical water vapour isotopic ratios, J. Geophys. Res., 115, D16116, doi:10.1029/2009JD013651, 2010. 27220, 27221, 27231

Galewsky, J., Sobel, A., and Held, I.: Diagnosis of subtropical humidity dynamics using tracers of last saturation, J. Atmos. Sci., 62, 3353–3367, 2005. 27222, 27229

García, O. E., Díaz, J. P., Expósito, F. J., Díaz, A. M., Dubovik, O., Derimian, Y., Dubuisson, P., and Roger, J.-C.: Shortwave radiative forcing and efficiency of key aerosol types using AERONET data, Atmos. Chem. Phys., 12, 5129–5145, doi:10.5194/acp-12-5129-2012, 2012. 27226

Gómez-Peláez, A., Ramos, R., and Pérez-de la Puerta, J.: Methane and carbon dioxide continuous measurements at Izaña GAW station (Spain), in: GAW Report (No. 168) of the "13th WMO/IAEA Meeting of Experts on Carbon Dioxide Concentration and Related Tracers Measurement Techniques (Boulder, Colorado, USA, 19–22 September 2005)", edited by: J. B. Miller, World Meteorological Organization (TD No. 1359), available at: http://www.wmo.int/pages/prog/arep/gaw/gaw-reports.html (last access: October 2014), 2006. 27225

Guirado, C., Cuevas, E., Cachorro, V. E., Toledano, C., Alonso-Pérez, S., Bustos, J. J., Basart, S., Romero, P. M., Camino, C., Mimouni, M., Zeudmi, L., Goloub, P., Baldasano, J. M., and de Frutos, A. M.: Aerosol characterization at the Saharan AERONET site Tamanrasset, Atmos. Chem. Phys., 14, 11753–11773, doi:10.5194/acp-14-11753-2014, 2014. 27223

James, P., Stohl, A., Spichtinger, N., Eckhardt, S., and Forster, C.: Climatological aspects of the extreme European rainfall of August 2002 and a trajectory method for estimating

the associated evaporative source regions, Nat. Hazards Earth Syst. Sci., 4, 733–746, doi:10.5194/nhess-4-733-2004, 2004. 27226, 27229
Kimberly, E. S.-C., Galewsky, J., Sharp, Z. D., and Dennis, K. J.: Deuterium excess in subtropical free troposphere water vapor: continuous measurements from the Chajnantor Plateau, northern Chile, Geophys. Res. Lett., 41, 8652–8659, doi:10.1002/2014GL062302, 2014. 27221
Millán, M. M., Salvador, R., Mantilla, E., and Kallos, G.: Photooxidant dynamics in the Mediterranean basin in summer: results from European research projects, J. Geophys. Res., 102, 8811–8823, 1997. 27228
Millán, M. M., Estrella, M., Sanz, M., Mantilla, E., Martín, M., Pastor, F., Salvador, R., Vallejo, R., Alonso, L., Gangotti, G., Ilardia, J., Navazo, M., Albizuri, A., Artiñano, B., Ciccioli, P., Kallos, G., Carvalho, R., Andrés, D., Hoff, A., Werhan, J., Seufert, G., and Versino, B.: Climatic feedbacks and desertification: the mediterranean model, J. Climate, 18, 684–701, 2004. 27228
Noone, D., Galewsky, J., Sharp, Z., Worden, J., Barnes, J., Baer, D., Bailey, A., Brown, D., Christensen, L., Crosson, E., Dong, F., Hurley, J., Johnson, L., Strong, M., Toohey, D., Van Pelt, A., and Wright, J.: Properties of air mass mixing and humidity in the subtropics from measurements of the D/H isotope ratio of water vapor at the Mauna Loa Observatory, J. Geophys. Res., 116, D22113, doi:10.1029/2011JD015773, 2011. 27221, 27225
Palmén, E. and Newton, C.: Atmospheric Circulation Systems: Their Structure and Physical Interpretation, Int. Geophys. Ser., 13, Academic Press, New York, 603 pp., 1969. 27222
Pierrehumbert, R.: Lateral mixing as a source of subtropical tropospheric water vapour, Geophys. Res. Lett., 25, 151–154, 1998. 27220
Prospero, J., Ginoux, P., Torres, O., Nicholson, S. E., and Gill, T. E.: Environmental characterization of global sources of dust with the Nimbus 7 total ozone mapping spectrometer (TOMS) absorbing aerosol product, Rev. Geophys., 40, 2-1–2-31, doi:10.1029/2000RG000095, 2002. 27228
Risi, C., Noone, D., Worden, J., Frankenberg, C., Stiller, G., Kiefer, M., Funke, B., Walker, K., Bernath, P., Schneider, M., Bony, S., Lee, J., Brown, D., and Sturm, C.: Process-evaluation of tropospheric humidity simulated by general circulation models using water vapour isotopic observations: 2. Using isotopic diagnostics to understand the mid and upper tropospheric moist bias in the tropics and subtropics, J. Geophys. Res., 117, D05304, doi:10.1029/2011JD016623, 2012. 27220

ACPD
15, 27219–27251, 2015

Rodríguez, S., González, Y., Cuevas, E., Ramos, R., Romero, P. M., Abreu-Afonso, J., and Redondas, A.: Atmospheric nanoparticle observations in the low free troposphere during upward orographic flows at Izaña Mountain Observatory, Atmos. Chem. Phys., 9, 6319–6335, doi:10.5194/acp-9-6319-2009, 2009. 27222, 27224, 27225, 27226

Rodríguez, S., Alastuey, A., Alonso-Pérez, S., Querol, X., Cuevas, E., Abreu-Afonso, J., Viana, M., Pérez, N., Pandolfi, M., and de la Rosa, J.: Transport of desert dust mixed with North African industrial pollutants in the subtropical Saharan Air Layer, Atmos. Chem. Phys., 11, 6663–6685, doi:10.5194/acp-11-6663-2011, 2011. 27223, 27228

Rodríguez, S., Alastuey, A., and Querol, X.: A review of methods for long term in situ characterization of aerosol dust, Aeolian Research, 6, 55–74, doi:10.1016/j.aeolia.2012.07.004, 2012. 27223, 27225

Rodríguez, S., Cuevas, E., Prospero, J. M., Alastuey, A., Querol, X., López-Solano, J., García, M. I., and Alonso-Pérez, S.: Modulation of Saharan dust export by the North African dipole, Atmos. Chem. Phys., 15, 7471–7486, doi:10.5194/acp-15-7471-2015, 2015. 27226, 27228

Rolph, G., Ngan, F., and Draxler, R.: Modeling the fallout from stabilized nuclear clouds using the HYSPLIT atmospheric dispersion model, J. Environ. Radioactiv., 136, 41–55, 2014. 27224

Schneider, M., González, Y., Dyroff, C., Christner, E., Wiegele, A., Barthlott, S., García, O. E., Sepúlveda, E., Hase, F., Andrey, J., Blumenstock, T., Guirado, C., Ramos, R., and Rodríguez, S.: Empirical validation and proof of added value of MUSICA's tropospheric δD remote sensing products, Atmos. Meas. Tech., 8, 483–503, doi:10.5194/amt-8-483-2015, 2015. 27221

Sodemann, H., Schwierz, C., and Wernli, H.: Interannual variability of Greenland winter precipitation sources: lagrangian moisture diagnostic and North Atlantic Oscillation influence, J. Geophys. Res., 113, D03107, doi:10.1029/2007JD008503, 2008. 27226, 27229

WMO: Guide to Meteorological Instruments and Methods of Observation, WMO Technical Publication No 8, World Meteorological Organisation, Geneva, 2008. 27234

ACPD
15, 27219–27251, 2015

Moisture pathways and H_2O-δD pairs in the subtropical North Atlantic free troposphere

Y. González et al.

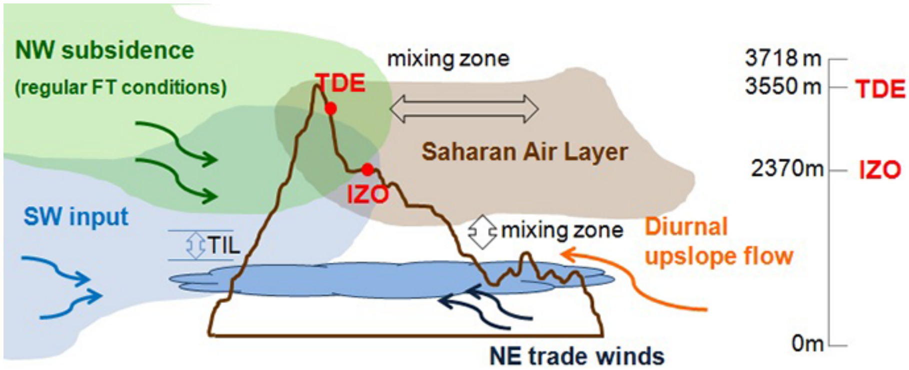

Figure 1. Schematic depiction of the processes influencing the water vapour balance over Tenerife Island in the subtropical North Atlantic. A temperature inversion layer (TIL) separates the Marine Boundary Layer (MBL) and the Free Troposphere (FT). In the MBL, NE trade winds blow, while in the FT, the regular NW subsidence regime is alternated in summer with Saharan dust outbreaks. At the island, the upslope winds prompt that MBL air reaches the low FT during daylight. IZO and TDE stations are represented as red dots.

ACPD
15, 27219–27251, 2015

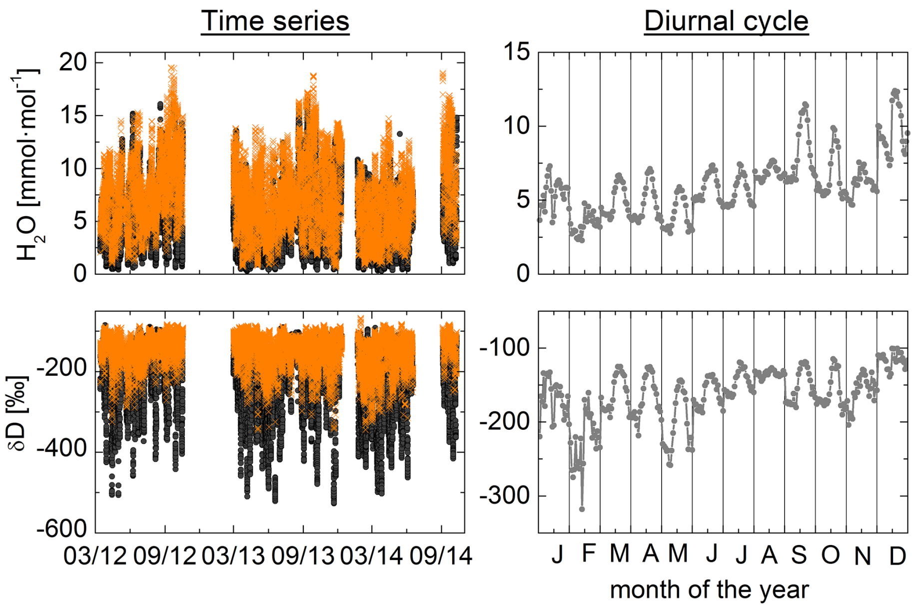

Figure 2. Left: time series of 10 min averages of H_2O and δD measured at IZO station. Black dots represent the data collected from midnight to 1 h after sunrise (nighttime). Orange crosses represent the data collected during daylight (from 3 to 10 h after sunrise). Right: monthly mean of the diurnal cycle of H_2O and δD.

ACPD
15, 27219–27251, 2015

Moisture pathways and H_2O-δD pairs in the subtropical North Atlantic free troposphere

Y. González et al.

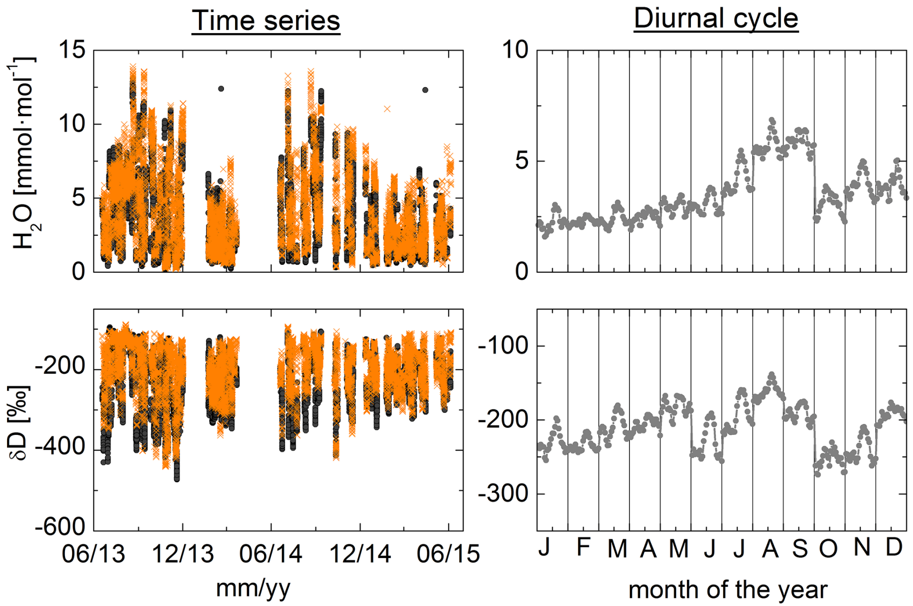

Figure 3. Same as Fig. 2 for data collected at TDE station.

Discussion Paper | Discussion Paper | Discussion Paper | Discussion Paper |

ACPD

15, 27219–27251, 2015

Moisture pathways and H_2O-δD pairs in the subtropical North Atlantic free troposphere

Y. González et al.

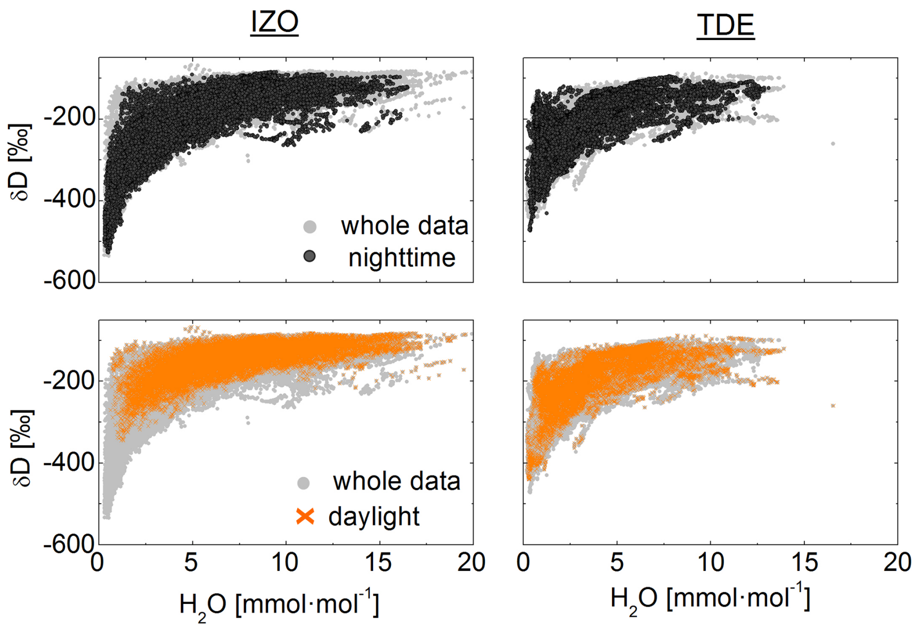

Figure 4. Distribution of the H_2O-δD pairs (10 min averages) at IZO (left) and TDE (right) stations. Grey dots show all data for the individual stations. Black dots represent the data collected during nighttime (from midnight to 1 h after sunrise). Orange crosses represent the data collected during daylight (from 3 to 10 h after the sunrise). The whole data set is presented in grey dots.

ACPD
15, 27219–27251, 2015

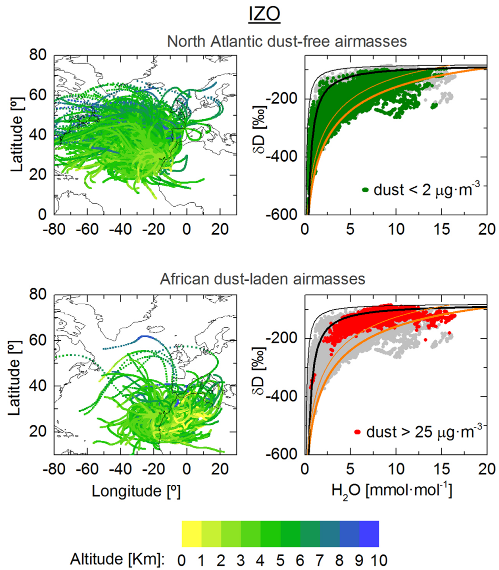

Figure 5. Airmasses reaching IZO station as a function of the dust load. First row shows non-dust conditions, second row, dust laden conditions. The colour-bar indicates the altitude (km) of these airmasses in each grid. The left column shows the trajectories. The right column shows the H_2O-δD distribution (pairs are presented on 10 min average): all data (grey dots), data measured under non-dust conditions (green dots) and data for dust laden conditions (red dots). Orange lines represent the evolution of an airmass that has experienced Rayleigh distillation for RH = 80 % and SST = 18 °C (thin line) and SST = 25 °C (thick line), respectively. These temperatures cover the annual mean sea surface temperatures around the Canaries. The black thin line represents the mixing between a moist airmass (initial conditions: H_2O = 18 mmol mol^{-1}, δD = −84 ‰) and a dry airmass (initial conditions: H_2O = 0.4 mmol mol^{-1}, δD = −600 ‰). The black thick line represents another mixing process (initial conditions for moist end member: H_2O = 16 mmol mol^{-1}, δD = −93 ‰; initial conditions for dry end member: H_2O = 0.4 mmol mol^{-1}, δD = −600 ‰).

ACPD
15, 27219–27251, 2015

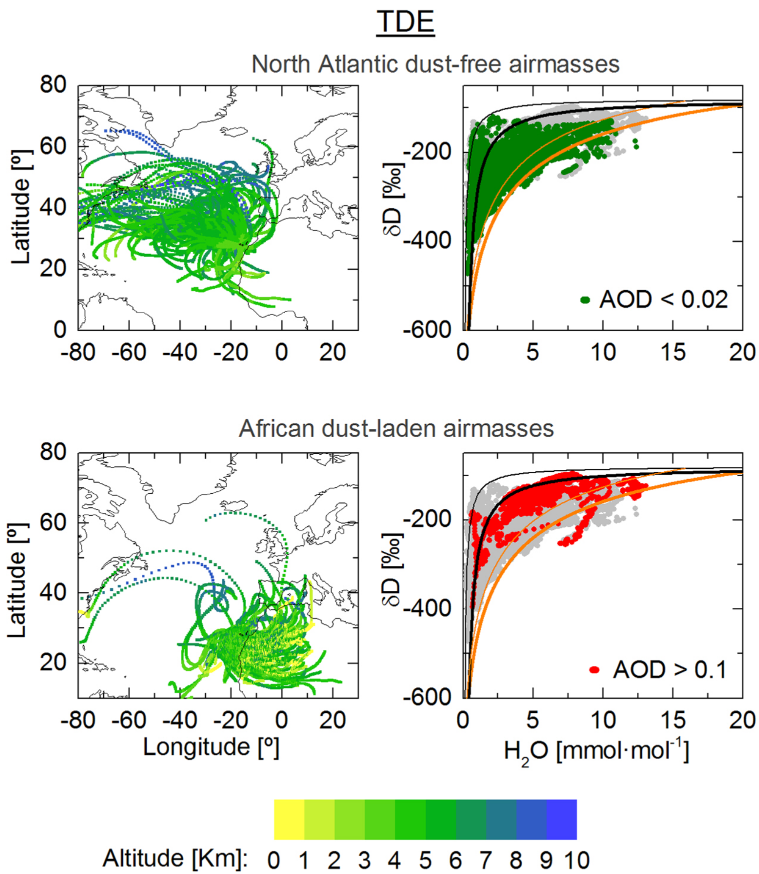

Figure 6. Same as Fig. 5 for the data collected at TDE station.

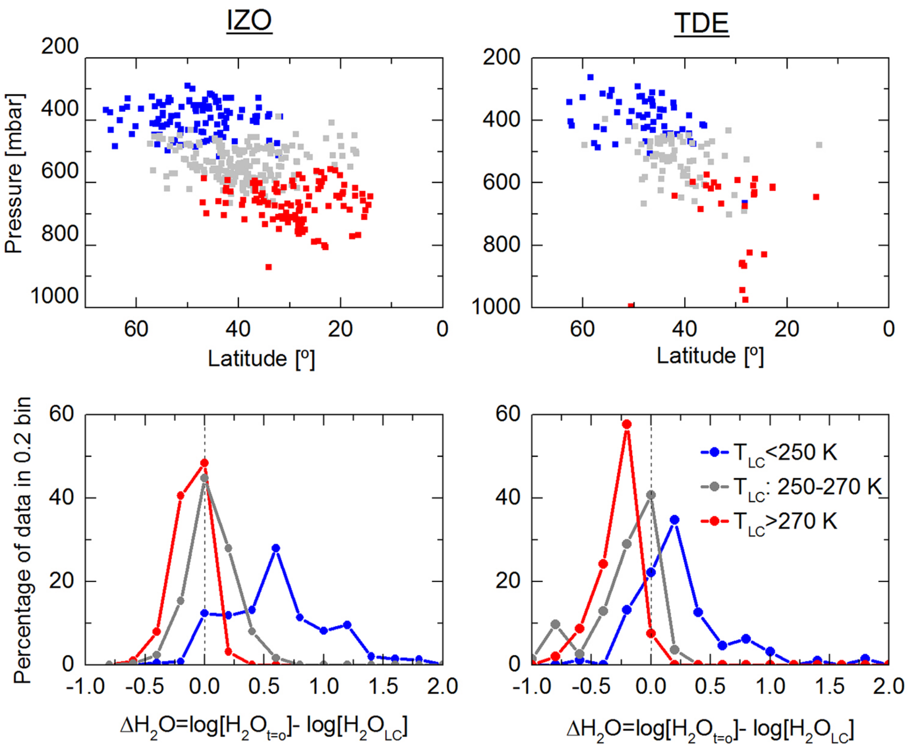

Figure 7. Trajectory-based analysis of the last condensation (LC) point for non SAL conditions. Upper panels: location (pressure-latitude) of LC point. Bottom panels: Histograms for $\Delta H_2O = \log[H_2O_{t=0}] - \log[H_2O_{LC}]$. The different colours correspond to different T_{LC} groups: $T_{LC} < 250$ K (blue line), 250 K < T_{LC} < 270 K (grey line) and $T_{LC} > 270$ K (red line).

ACPD
15, 27219–27251, 2015

Moisture pathways and H_2O-δD pairs in the subtropical North Atlantic free troposphere

Y. González et al.

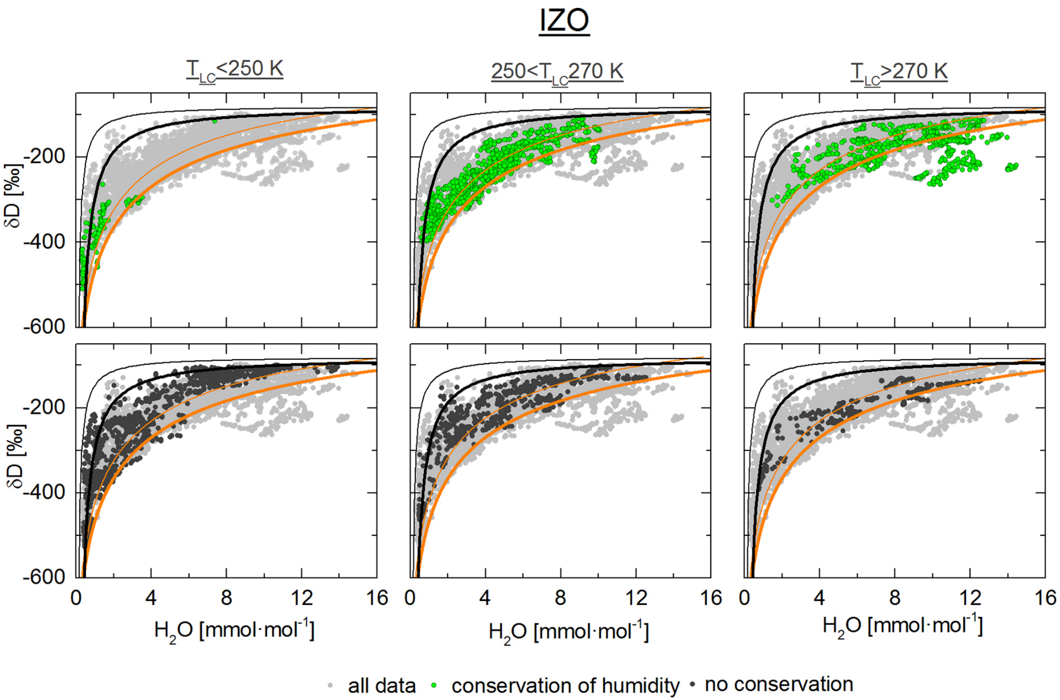

Figure 8. H_2O-δD distribution (10 min data within ±3 h of the arrival time of the airmass) measured at IZO station and analysed with regard to the LC point. The data set has been grouped in 3 groups corresponding to different condensation temperatures: $T_{LC} < 250$ K, 250 K $< T_{LC} <$ 270 K and $T_{LC} > 270$ K. The H_2O-δD pairs measured for reduced mixing since LC ($\Delta H_2O \pm 0.1$) are presented in green. Pairs measured for increased mixing since LC (ΔH_2O outside ±0.1) are presented in dark grey. Rayleigh and mixing curves are plotted as in Figs. 5 and 6.

ACPD
15, 27219–27251, 2015

Moisture pathways and H_2O-δD pairs in the subtropical North Atlantic free troposphere

Y. González et al.

Title Page
Abstract | Introduction
Conclusions | References
Tables | Figures
◂ | ▸
Back | Close
Full Screen / Esc
Printer-friendly Version
Interactive Discussion

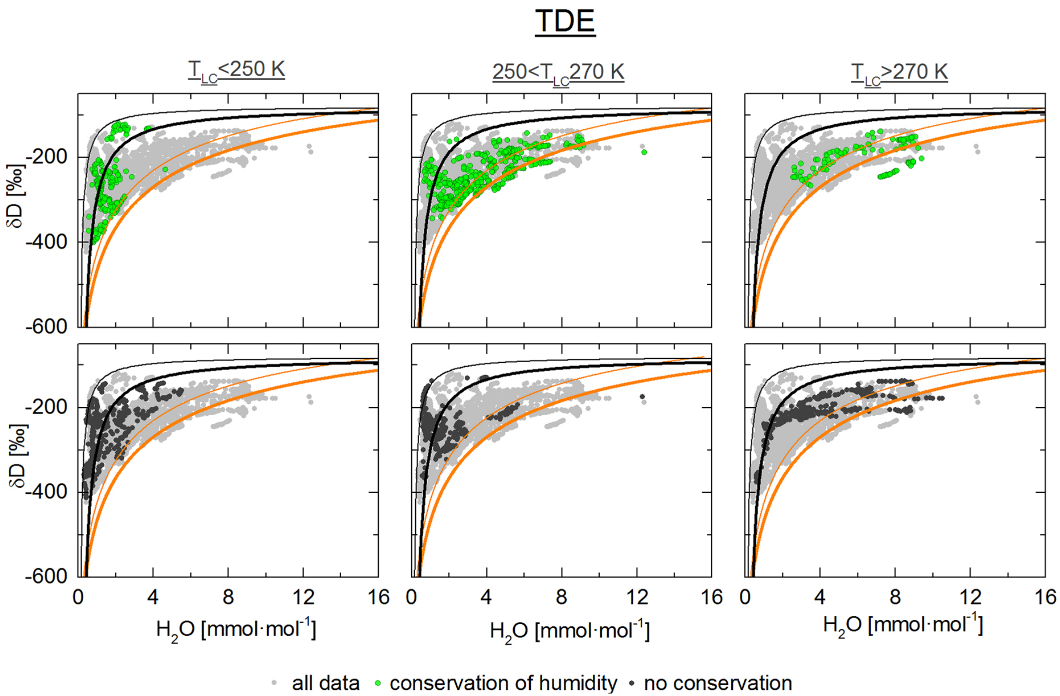

Figure 9. Same as Fig. 8 for the data collected at TDE station.

ACPD
15, 27219–27251, 2015

Moisture pathways and H_2O-δD pairs in the subtropical North Atlantic free troposphere

Y. González et al.

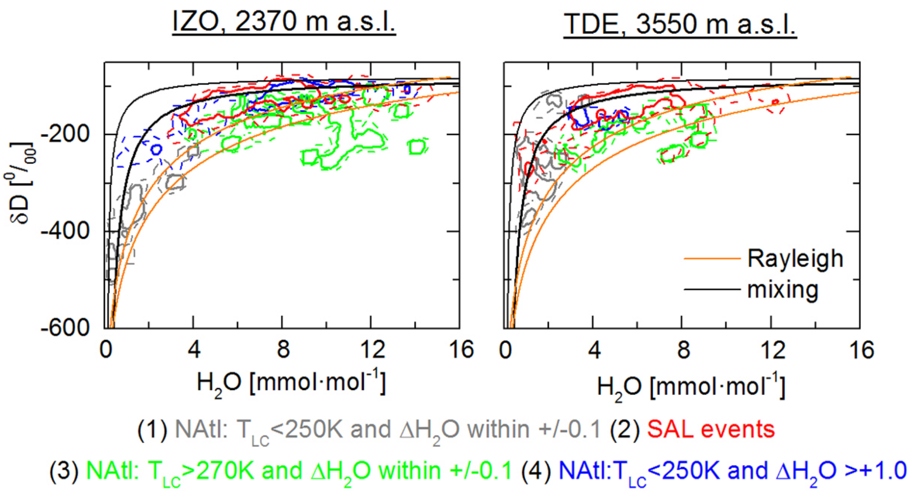

Figure 10. H_2O-δD distributions as obtained for the four different moisture pathways that determine the free troposphere moisture budget in the surroundings of Tenerife (Left panel for IZO and right panel for TDE). Depicted are contour lines indicating the areas of the highest data point density. The thin dashed and thick solid lines mark the areas that include 95 and 66 % of all data, respectively. The different colour of the contour lines mark the different pathways (1–4) as given in the legend. Rayleigh and mixing curves are plotted as in Figs. 5, 6, 8 and 9.

ACPD
15, 27219–27251, 2015

Moisture pathways and H_2O-δD pairs in the subtropical North Atlantic free troposphere

Y. González et al.

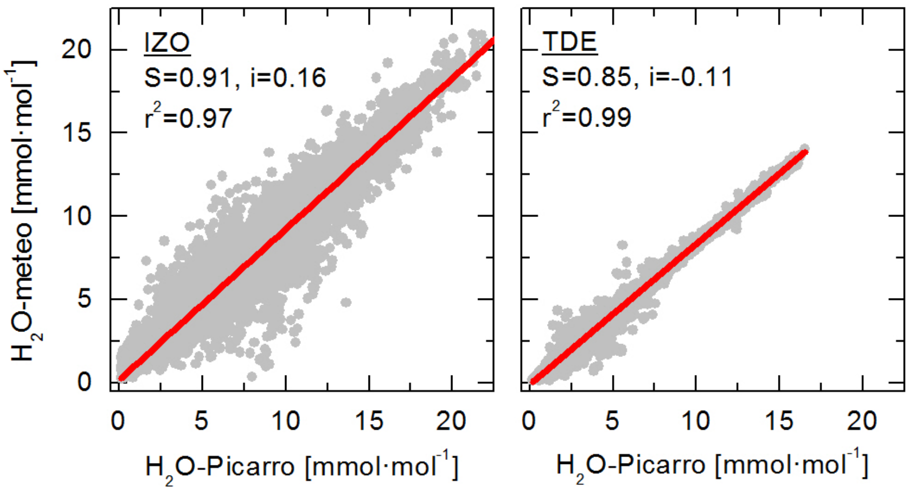

Figure A1. Grey dots show the 10 min humidity data pairs of the Picarro and the meteorological at IZO and TDE. Red lines indicate the linear fit of the distribution. S = slope, i = intercept, r^2 = coefficient of determination.

ACPD
15, 27219–27251, 2015

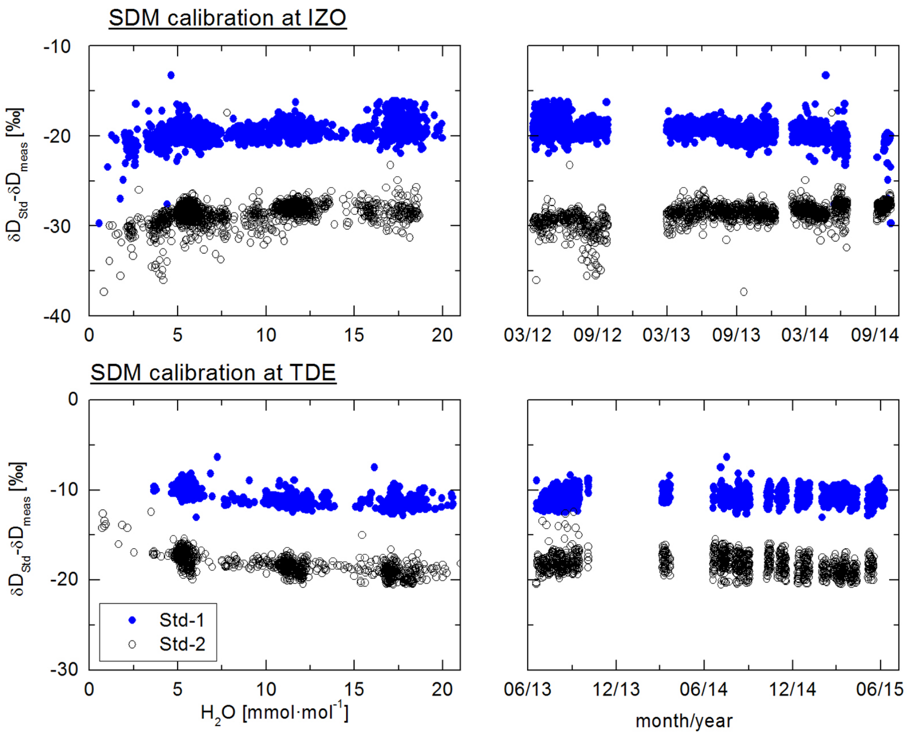

Figure A2. Difference between the measured δD and that from the two liquid standards used for calibrating the instruments at IZO (first row) and TDE stations (second row). The left column depicts the dependence of this difference to the humidity during calibration. The right column shows the evolution of the difference with the time for all humidity levels.

ACPD
15, 27219–27251, 2015